

Adaptive Two-Channel Automatic Gain Control System

Alexander Utter, Henry Chen, Shane Ouchi, David Money Harris, Amanda Rainer, Keane Kaneakua, and Chris Prounh
 Harvey Mudd College
 301 Platt Blvd.; Claremont, CA 91711-5901
 909-607-3623
 autter@hmc.edu, hchen@hmc.edu, souchi@hmc.edu,
 harris@hmc.edu, arainer@hmc.edu,
 kkaneakua@hmc.edu, cprounh@hmc.edu

Samuel S. Osofsky
 The Aerospace Corporation
 2350 E. El Segundo Blvd.; El Segundo, CA 90245-4691
 310-336-5886
 Samuel.S.Osofsky@aero.org

Abstract—A new method is proposed for enhancing the performance of automatic gain control systems coupled with analog-to-digital converters (ADCs). This approach is focused on increasing the dynamic range of software-defined radios in applications where high data rates and low-power requirements make increasing ADC resolution impractical. This novel approach utilizes two input channels in order to aggressively enhance sensitivity while remaining responsive to rapid changes in input signal power. For modest rates of input power change, signal-to-error-power ratios (SER) can be enhanced by 6 dB or more. A methodology for selecting control parameters, algorithms for adjusting to input characteristics in real time, and results from a functional prototype are discussed.^{1,2}

number, the analogy is still useful for labeling each output. In other applications, constant scaling factors do not disrupt the signal, and this gain-compensation step can be removed as long as the gain change is sufficiently slow.

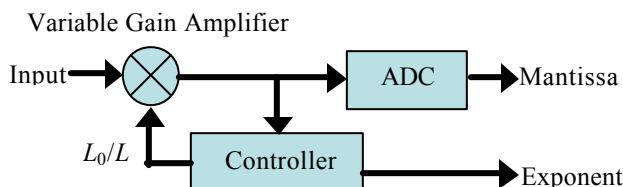


Figure 1: Traditional automatic gain control (AGC)

TABLE OF CONTENTS

1. INTRODUCTION.....	1
2. SIGNAL-TO-ERROR RATIO.....	2
3. TWO-CHANNEL AUTOMATIC GAIN CONTROL	2
4. ADAPTING TO INPUT SIGNAL TYPE.....	4
5. PROTOTYPE.....	6
6. CONCLUSIONS	7
7. REFERENCES	8
8. BIOGRAPHIES	8

1. INTRODUCTION

Automatic gain control (AGC) systems increase dynamic range by applying a variable gain to an input signal prior to quantization, in an attempt to place the resulting amplified or attenuated signal at the optimal input power for the ADC. The resulting dynamic range is limited by the range of the variable gain amplifier (VGA) and the controller’s ability to select the optimal gain setting. Several types of AGC topologies exist to address the latter concern. The most common topology, shown in Figure 1, uses a closed loop controller to adjust gain such that the output power matches a predefined set-point. In this figure, the bare ADC has a full scale of $\pm L_0$, and the effective full scale of the entire assembly is $\pm L$. In some configurations, the output from the ADC is digitally multiplied by an attenuation factor equal to the applied gain [2]. The controller indicates the applied gain using the “exponent” output. Although the format of the mantissa and exponent may not be a literal floating point

If input power is constant, then the ideal set-point is the one that produces the optimal SER as discussed above. However, since all control systems have associated delays, and the SER penalty for having excessive gain (saturation) is much higher than the penalty for inadequate gain (potential for marginally better SER), it is useful to include a safety margin.

For very high rates of change in input signal power, these safety margins can become prohibitively large. Saturation is avoided for worst-case scenarios, but at the cost of drastic reductions in SER for constant power signals. One alternative topology that addresses this problem is the full multichannel AGC system shown in Figure 2 [3][4][5]. By providing a bank of fixed gains and automatically selecting the highest-gain unsaturated channel, it can apply optimal gain settings on a sample-by-sample basis. This topology is especially useful for capturing transient signals in which the peak amplitude is difficult to predict. Typically, fixed gains are set at a spacing of $2x$, to minimize worst-case loss of precision, but this requires rapidly increasing system complexity for a limited increase in dynamic range. Increasing channel spacing increases the dynamic range gained per additional channel, but decreases expected SER. Although this type of AGC system is uniquely immune to even the most rapid input power changes, its cost and complexity are prohibitive for many applications.

¹ 0-7803-9546-8/06/\$20.00© 2006 IEEE

² IEEEAC paper #1113, Version 1, September 2, 2005

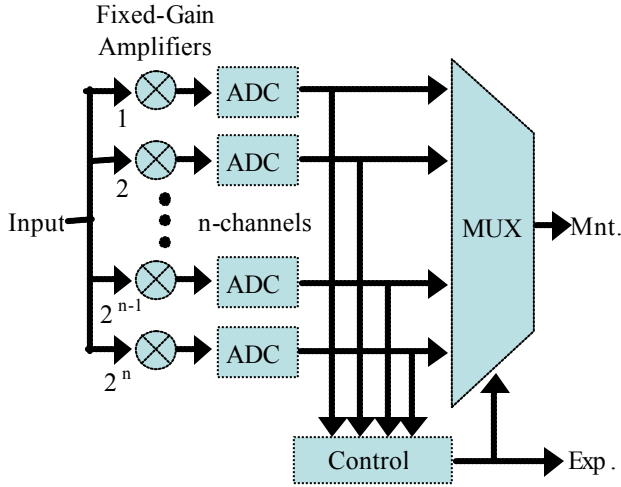


Figure 2: Full multichannel AGC

Another class of systems for increasing ADC dynamic range consists of iterative and sub-ranging digitization techniques, which use a pipeline of comparators and ADCs to acquire increasingly precise digitized data [6]. The net effect is equivalent to additional output bits. Iterative methods are primarily limited by accumulated analog error. Other methods include companding and other nonuniform quantization methods [7]. These methods use variable spacing between each output code to provide increased detail in critical input ranges. They are most effective when characteristics of the input signal are well defined and the ADC is not required to handle strong interfering signals. Fortunately, they can usually be combined effectively with AGC systems, so a detailed discussion is beyond the scope of this paper.

This paper introduces an adaptive two-channel AGC system. We begin by formally defining the signal-to-error ratio. We then present the novel system and explain how to choose the best gain settings at any power level for a number of signal types. Next, we present an algorithm for detecting and adapting to each of these signal types in real time. Finally, a prototype hardware implementation demonstrates proof of concept. We demonstrate that the improved system offers at least 6 dB better SER than a conventional single-channel AGC for signals with moderate rates of input power change.

2. SIGNAL-TO-ERROR RATIO

For all ADCs, the quantization process inherently introduces error into a signal. The SER can be maximized by increasing signal power well above the fixed-power “noise” introduced by rounding to the nearest output code, while avoiding the distortion error caused by saturation effects. For common bounded input-types such as sinusoids or uniform noise, the optimal input power is intuitively just below the point at which saturation begins. For unbounded inputs such as Gaussian noise, the input power that maximizes SER for a given probability density function

(PDF) can be found by calculating expected error power [1], as shown in Equation 1,

$$E(q^2 | L, A) = \int_{-\infty}^{+\infty} p(x, A) q(x, L)^2 dx \quad (1)$$

where $E(q^2 | L, A)$ is the expected error power for a given nonsaturated ADC range of $\pm L$ and a given input power A , $p(x, A)$ is the input signal’s probability density function, and $q(x, L)$ is the quantization error for a given input x . To a reasonable approximation under normal conditions, quantization error for an ADC with uniform output code spacing can be expressed as in Equation 2,

$$q(x, L)^2 \approx \begin{cases} \frac{1}{12} Q^2 & |x| \leq L \\ (|x| - (L - \frac{1}{2}Q))^2 & |x| > L \end{cases} \quad (2)$$

where $Q = 2L / 2^N$ is the distance between output codes for an ADC with N output bits. Note that for any given quantity L / A , the input power A^2 and the expected error power $E(q^2 | L, A)$ are proportional to each other. Therefore, these results can be generalized by expressing SER as a function of L / A . The optimal value for this ratio can then be read off the peak of a plot like the one shown in Figure 3. The width of the “triangle” in this type of figure also shows the system’s input dynamic range—the range of input power for which output power exceeds error power by an acceptable margin.

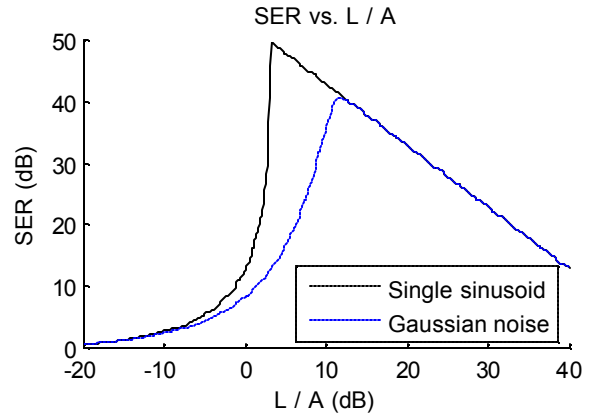


Figure 3: Expected SER vs. ADC scale relative to input power for two different PDFs

3. TWO-CHANNEL AUTOMATIC GAIN CONTROL

The novel two-channel AGC topology shown in Figure 4 is a hybrid of traditional and full multichannel automatic gain control, with an intermediate tradeoff between system complexity and ability to respond to rapid changes in input power. Qualitatively, the two channels allow the system to simultaneously use both an aggressive gain for maximum precision and a conservative gain with a wide safety margin for catching outliers.

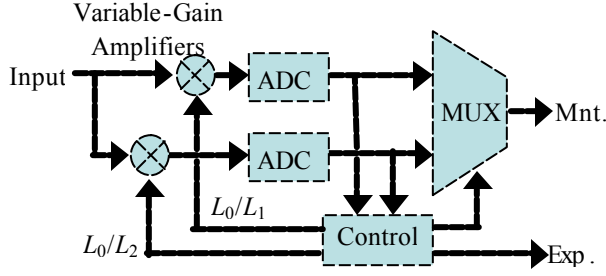


Figure 4: Adaptive two-channel AGC

Optimal gain settings can be chosen to maximize the expected SER for a given estimated variation in input power. To account for potential variation in the input power A , an additional integral is required as shown in Equation 3,

$$E(q^2 | L_1, L_2, \hat{A}, \mathbf{s}_A) = \int_0^{+\infty} p_A(A | \hat{A}, \mathbf{s}_A) \left[\int_{-\infty}^{+\infty} p(x, A) q(x, L_1, L_2)^2 dx \right] dA \quad (3)$$

where $\pm L_1$ and $\pm L_2$ are the ranges for each channel's ADC ($L_1 > L_2$), \hat{A} is the best estimate or prediction of the instantaneous signal power, \mathbf{s}_A is a rate of change parameter whose meaning depends on the chosen function p_A , and the function $p_A(A | \hat{A}, \mathbf{s}_A)$ is the probability density of receiving an actual input power A given \hat{A} and a change rate \mathbf{s}_A . In many systems the value of \hat{A} changes slowly with time, such that the best estimate of its value in the near future is simply the most recent estimate of input signal power. However, there will always be some time lag between a change in input power, a corresponding change in the estimated power, and the control system's selection of new gain settings. By allowing for random variation in input power with respect to predicted input power, this model takes into account both uncertainty in the predicted power level and the maximum rate of change with respect to the control system's time delay. Depending on the application and the nature of the expected signal, different p_A functions may be appropriate.

For this model, p_A is a Gaussian distribution in logarithmic space, such that 68% of all A fall within $\pm s_A$ dB of \hat{A} . In this distribution, there is an equal chance of an input power increase to 200% of \hat{A} (+6 dB) or a decrease to 50% of \hat{A} (-6 dB), and the maximum possible input power is unbounded. The expression for this distribution is given in Equation 4,

$$p_{A,dB}(A_{dB} | \hat{A}, \mathbf{s}_A) = \frac{1}{\mathbf{s}_A \sqrt{2\pi}} \exp \left[-\frac{1}{2} \left(\frac{A_{dB}}{\mathbf{s}_A} \right)^2 \right] \quad (4)$$

where $A_{dB} = 20 \log_{10}(A / \hat{A})$. To perform the necessary integration, this function must be converted to give the appropriate probability density as a function of A in linear space. The linearized probability density is given by Equation 5.

$$p_A(A | \hat{A}, \mathbf{s}_A) = \frac{20}{A/\hat{A} \ln(10)} \frac{1}{\mathbf{s}_A \sqrt{2\pi}} \exp \left[-\frac{1}{2} \left(\frac{20 \log_{10} A/\hat{A}}{\mathbf{s}_A} \right)^2 \right] \quad (5)$$

In the two channel system, some method must be devised to combine the information from both channels. Expected error for each channel is given by Equation 2. In the case where both channels are not saturated, then expected error is proportional to Q_1^2 and Q_2^2 , respectively. Since Q is directly proportional to L , and we can assume $L_1 \gg L_2$, the low-gain channel L_1 contributes almost nothing in this case. In this region, we should simply use the output of the high-gain channel. Once the high-gain channel saturates, however, its expected error increases so rapidly that only the output from the low-gain channel should be used. This method of combining the two channels gives the estimated error function $q(x)^2$ shown in Equation 6.

$$q(x, L_1, L_2)^2 \approx \begin{cases} \frac{1}{12} Q_2^2 & |x| < L_2 \\ \frac{1}{12} Q_1^2 & L_2 \leq |x| \leq L_1 \\ (|x| - (L_1 - \frac{1}{2} Q_1))^2 & L_1 < |x| \end{cases} \quad (6)$$

If $L_2 = 0$, this system is equivalent to a traditional single-channel AGC, so no changes are required to re-derive optimal safety margins for the single-channel system as a function of \mathbf{s}_A .

SER-optimizing input power levels can be found by numeric integration. Results for an input PDF corresponding to a sinusoid are shown in Figure 5. As one might expect, optimal ADC scale relative to signal power increases with variation in input power for both topologies. Optimal scale for the single-channel system lies between the scale for each channel of the two-channel system, such that $L_2 < L = L_1$ in all cases.

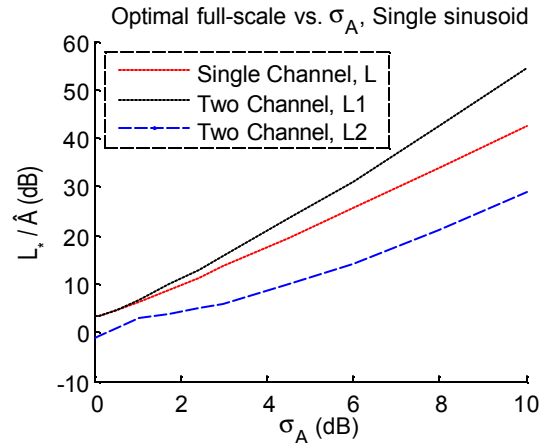


Figure 5: Optimal ADC scale vs. \mathbf{s}_A , sinusoidal input.

A full plot of SER vs. L_1 and L_2 for a Gaussian input with $\mathbf{s}_A = 3$ dB is shown in Figure 6. Note that the cross sections at extreme L_1 and L_2 values are identical to the curve in Figure 5.

3, but the two channels act synergistically near the overall maximum. This synergistic peak becomes larger as variation in input power increases, and its height gives the expected improvement in SER for a two-channel system. This expected improvement in SER is shown in Figure 7 for a variety of input PDF choices; as expected, improvement increases with s_A . For all selected PDFs, SER improvement exceeds 6 dB for all $s_A > 3$ dB.

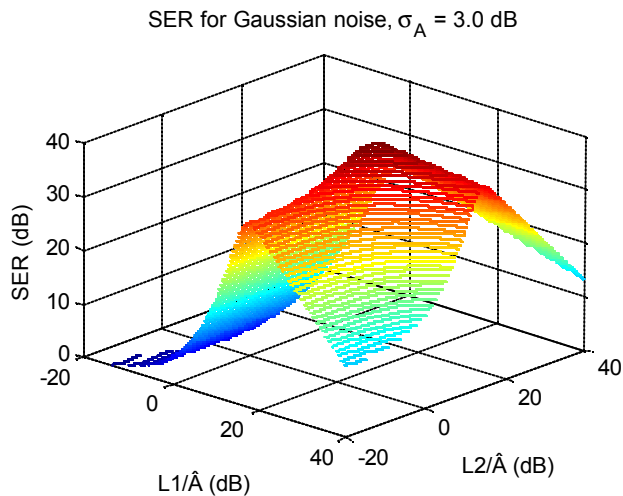


Figure 6: SER vs. L_1 and L_2 , Gaussian input

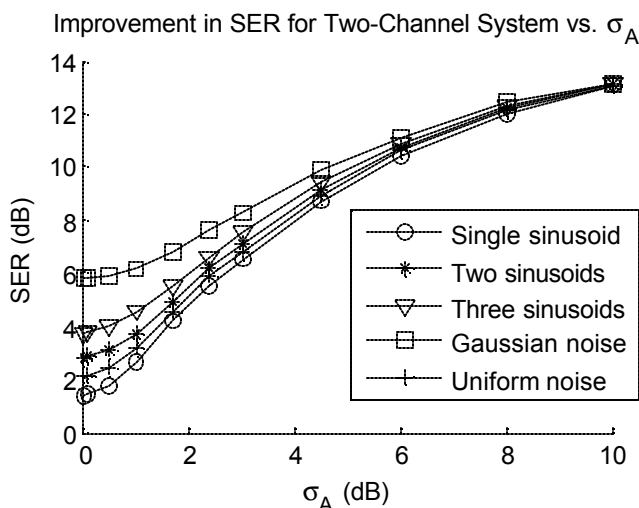


Figure 7: SER improvement for two-channel AGC

Calibration mismatch between the two channels is a serious potential problem for the two-channel AGC system. Careful attention must be paid to minimize or compensate for any differences that could cause distortion as the output is switched from one ADC to the other, such as DC offset, VGA gain error, and ADC scale mismatch. In the case when neither channel is saturated, we can model these three effects as shown in Equation 7:

$$\begin{aligned} y_1 &= A_1 x + D_1 + n_1 \\ y_2 &= A_2 x + D_2 + n_2 \end{aligned} \quad (7)$$

where x is the input signal, y_x is the output of each channel after compensation for the nominal VGA gain, A_x is the scalar error caused by VGA gain error and ADC scale mismatch, D_x is the DC offset for each channel, and n_x accounts for all quantization error and other zero-mean noise. Solving for y_2 in terms of y_1 yields Equation 8.

$$y_2 = \frac{A_2}{A_1} y_1 + \left(D_2 - \frac{A_2}{A_1} D_1 \right) + \left(n_2 - \frac{A_2}{A_1} n_1 \right) \quad (8)$$

Solving for the least-squares best fit line gives Equation 9.

$$\begin{aligned} \frac{A_2}{A_1} &\approx \frac{\sum (y_1 - \bar{y}_1)(y_2 - \bar{y}_2)}{\sum (y_1 - \bar{y}_1)^2} \\ \Delta D &= \left(D_2 - \frac{A_2}{A_1} D_1 \right) \approx \bar{y}_2 - \frac{A_2}{A_1} \bar{y}_1 \end{aligned} \quad (9)$$

This allows an entirely digital algorithm for compensating for the differences between channels. Since the relevant error values are likely to change each time new gain settings are applied, it would be useful to calculate estimates in real time. We can accomplish this by implementing an appropriate accumulating average or Kalman-filter estimator for the expressions given in Equation 9 taking care to average only those points for which neither channel is saturated. The final step is to select one channel as a reference and adjust the output of the other channel to match it. If we arbitrarily choose channel 2 to be the reference, then the compensated output for channel 1 is given by Equation 10.

$$y_1' = A_2 x + D_2 = \frac{A_2}{A_1} y_1 + \Delta D \quad (10)$$

The two-channel topology is also compatible with companding and other nonuniform quantization techniques. Although the presented derivation of optimal gain coefficients assumes uniform ADC quantization and symmetric channels, re-deriving coefficients for other ADC types merely requires the insertion of the appropriate function $q(x)$. If desired, each channel could have different quantization functions, although this would require a more sophisticated method of selecting the most appropriate channel or combining output from both channels.

4. ADAPTING TO INPUT SIGNAL TYPE

The method discussed in Section 2 allows the derivation of optimal gain settings for each channel for a particular input PDF, but the resulting coefficients change with input type. In many radio receivers, the input PDF cannot be accurately predetermined, because multiple transmitters and interference sources can switch on and off while the receiver is running. Therefore, some method of detecting the input signal type is required so that the AGC system can apply the appropriate gain settings.

Let us assume that each received primary and interfering signal can be modeled as a sinusoid with random relative frequency and phase. The input distribution for a single sinusoid is given by Equation 11.

$$p(x, A) = \frac{1}{A\sqrt{2}} \left(1 - \left(\frac{x}{A\sqrt{2}} \right)^2 \right)^{\frac{1}{2}} \quad (11)$$

Since summation of two signals is equivalent to convolution of their PDFs, we can find the PDF for the sum of any number of equal-power sinusoids numerically. The results, after renormalization to an RMS power of 1.0, are shown in Figure 8. Note that the sum of an infinite number of such sinusoids approaches a Gaussian distribution as described by the Central Limit Theorem. For this reason, the impact on optimal gain coefficients due to each additional sinusoid becomes very small after the third. Therefore, the consideration of these four PDFs is adequate for this model.

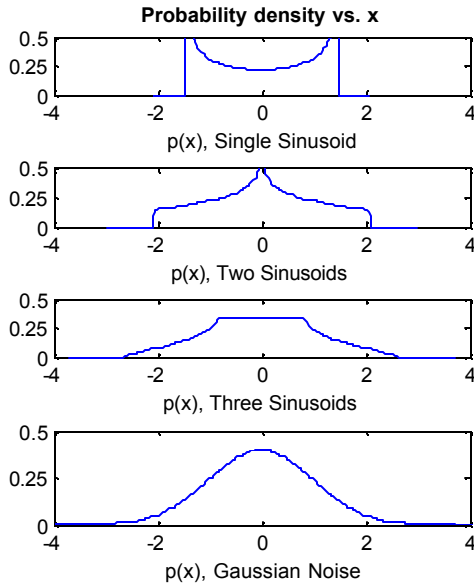


Figure 8: Sinusoid-derived input PDFs

While the uniform distribution is not sinusoid-derived, it has been included in later analyses because it is useful in many applications. Results for this set of five PDFs are listed in Table 1 and Table 2. Note that the optimal gain coefficients for both the single- and two-channel systems can vary by up to 10 dB, depending on the input PDF, further emphasizing the need for an adaptive controller.

Table 1: Optimal scale coefficients for $s_A = 0$

Input PDF	One Ch.	Two Channels	
	L/\hat{A} (dB)	L_1/\hat{A} (dB)	L_2/\hat{A} (dB)
Single sinusoid	+3.3	+3.3	-1.0
Two sinusoids	+6.4	+6.5	+0.7
Three sinusoids	+8.2	+8.3	+1.8
Gaussian	+11.9	+13.0	+4.7
Uniform	+4.8	+4.8	+0.0

Table 2: Optimal scale coefficients for $s_A = 3$ dB

Input PDF	One Ch.	Two Channels	
	L/\hat{A} (dB)	L_1/\hat{A} (dB)	L_2/\hat{A} (dB)
Single sinusoid	+13.7	+15.7	+6.1
Two sinusoids	+15.7	+18.0	+7.6
Three sinusoids	+16.7	+19.1	+8.0
Gaussian	+17.7	+20.7	+8.3
Uniform	+14.5	+16.6	+6.6

While kurtosis might be an excellent candidate for distinguishing between input distributions, it is too computationally intensive for most real-time, high data-rate applications. A very easily implemented alternative is the single-bin histogram given in Equation 12,

$$ZBX = \frac{1}{N} \sum_{n=1}^N \begin{cases} 1, & |x_{[n]}| < b * RMS \\ 0, & otherwise \end{cases} \quad (12)$$

where ZBX (Zero Bin $X_{[n]}$) is the fraction of $x_{[n]}$ that fall near zero, in a bin size that is a fraction b of the current estimated RMS power. A simple Kalman estimator for ZBX can be formulated as shown in Equation 13,

$$ZBX_{[n+1]} = ZBX_{[n]} + a_{ZBX} \times \left(\begin{cases} 1, & |x_{[n]}| < b * RMS_{[n]} \\ 0, & otherwise \end{cases} - ZBX_{[n]} \right) \quad (13)$$

where a_{ZBX} is the update-rate coefficient. A large a_{ZBX} will allow the estimator to respond to changes in the input distribution more quickly, but will reduce the effective averaging period and therefore increase noise. The appropriate choice is the largest value that still allows the system to accurately distinguish between input types. Simulated tests show that, qualitatively, a value on the order of 1/256 is sufficiently accurate without being excessively slow. This particular value has the added benefit of removing the need for an integer or floating point multiplier in the controller hardware. The remaining parameter, b , should be chosen to maximize the difference between expected ZBX values for potential input distributions. Figure 9 shows a plot of expected ZBX vs. b for the five input distributions under consideration. In this case, a value of $b = 1.0$ is an excellent choice for distinguishing these five distributions because the spacing is adequate and because this threshold maintains a strictly increasing mapping of ZBX to the optimal L/\hat{A} coefficients for the distributions listed in Table 1 and Table 2.

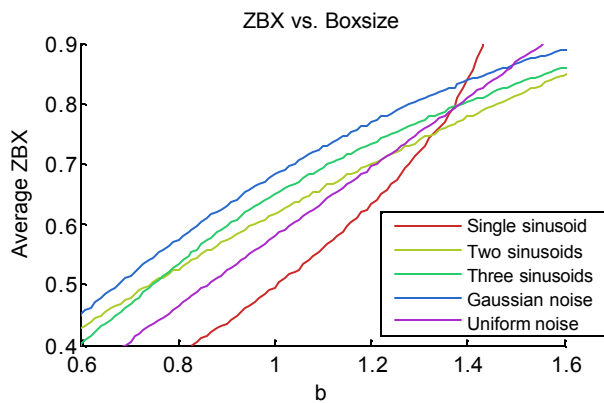


Figure 9: Expected ZBX vs. b

Since the mapping of ZBX to optimal gain is smooth when gains are expressed logarithmically, linear interpolation in log-space seems to be a safe choice for selecting gain coefficients for intermediate ZBX values. (A statistical analysis to determine precisely optimal coefficients given a PDF of expected ZBX for each selected distribution is well beyond the scope of this paper.) The best choice when ZBX falls outside the expected range is not as clear. For the given ZBX estimator, extremely high ZBX values may indicate that the RMS estimate is erroneously high. This could be caused by a sudden drop in input power if the ZBX estimator is faster than the RMS power estimator, and gain coefficients could be set very low in response to this indicator. Similarly, for fast ZBX estimators, low ZBX may indicate a sudden increase in input signal power. Unfortunately, the high precision required to accurately distinguish between input distributions makes it likely that the RMS power estimator will be able to respond more

quickly than the ZBX estimator, so extreme ZBX values may or may not reveal useful information.

5. PROTOTYPE

A prototype of the adaptive two-channel AGC system was constructed to demonstrate successful application of the theory. The prototype contained an on-board Analog Devices AD9726 16-bit DAC (Digital-to-Analog Converter) for generating test waveforms, plus a pair of Analog Devices AD9480 8-bit ADCs capable of operating at 250 MSPS. High sampling rates were desired primarily as a demonstration of the theory's frequency-independence. Data processing and control were implemented using a Xilinx Spartan 3 FPGA.

A block diagram for the AGC system is shown in Figure 10. The main input is from the two ADCs, whose data clocks may have a significant but constant phase offset. After synchronization to the primary clock domain, each sample from the high gain channel is checked for clipping. If that output is saturated, the other channel is selected. The selected channel's sample is multiplied by that channel's current full scale to obtain a single normalized 16-bit data stream, which is recorded to RAM to compare to the original test waveform. Simultaneously, an observer tracks RMS power and ZBX using a pair of nonlinear Kalman estimators. The ZBX coefficient is queried against a lookup table to determine the optimal gain coefficients for each channel, which are multiplied by the current estimated RMS power (\hat{A}) to obtain the optimal full scale for each channel (L_1, L_2). Finally, these values are fed to a controller for the pair of variable gain amplifiers, which updates the gain

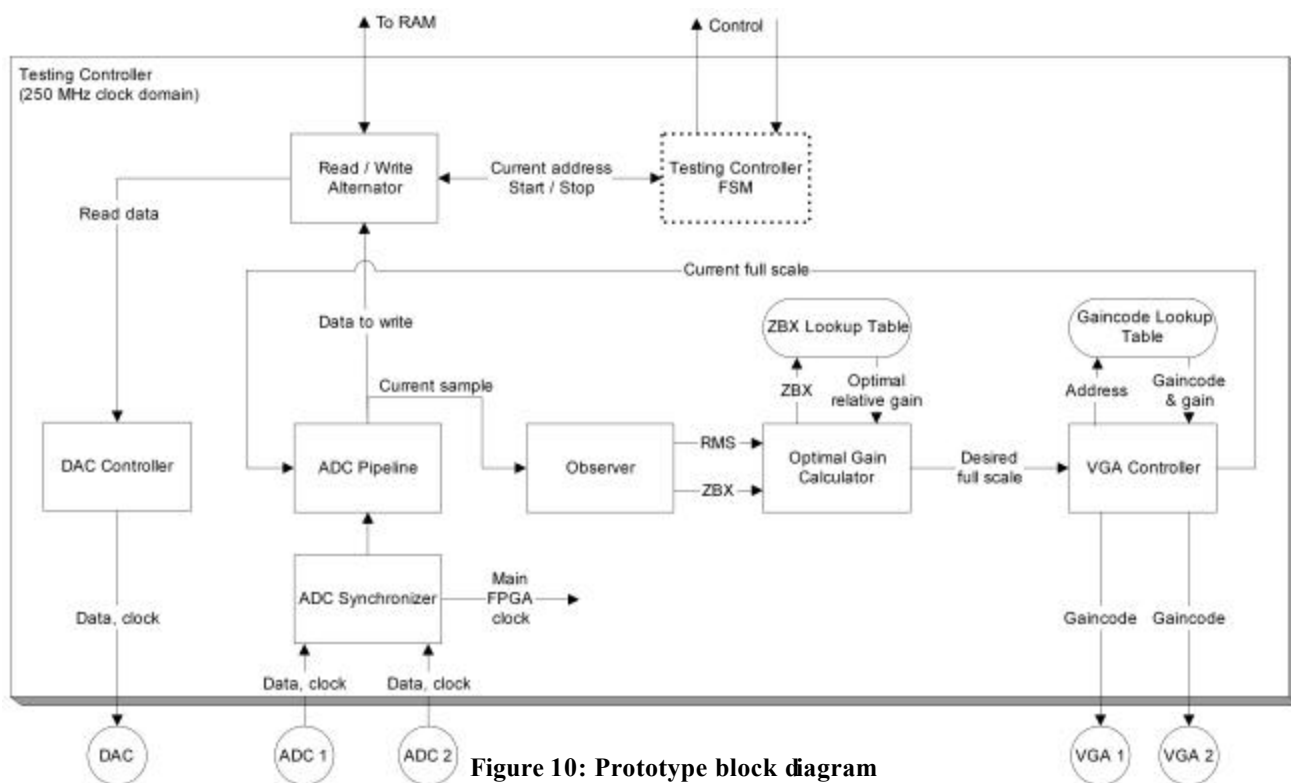


Figure 10: Prototype block diagram

settings as often as possible, and keeps track of the current setting for proper normalization of input samples.

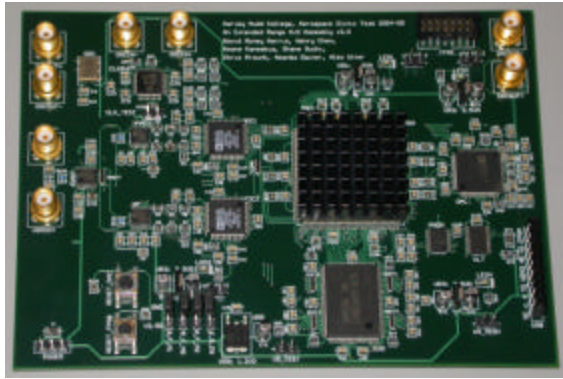


Figure 11: Photo of prototype

The current version of the prototype, shown in Figure 11, is functional. A typical test input consists of a series of brief segments, where each segment contains the sum of one or more sinusoids of random frequency and phase. In the simplest such test, the total power of each segment decreases exponentially from 0 to -96dB . An excerpt from this waveform is shown in Figure 12.

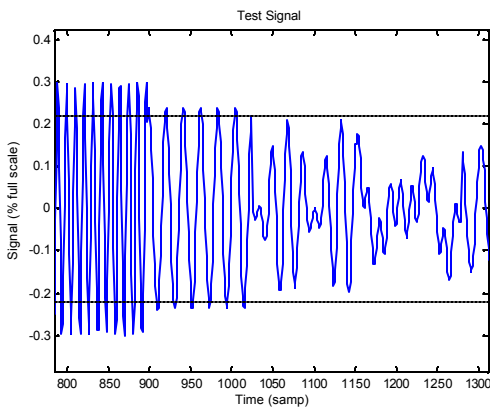


Figure 12: Subset of typical test input

The test can be considered successful if it reasonably matches predicted results for SER vs. input power. In an ADC with no automatic gain-control system, this curve should look like the “triangle” in Figure 3. An ideal AGC will apply exactly the gain or attenuation needed to shift the effective input power to the optimal point on this curve. This will produce a flat region whose width is equal to the dynamic range of available VGA gain, and normal falloff beyond this region.

Figure 13 shows the prototype test results for a fixed-gain dual-channel configuration like the one shown in Figure 2. Testing was performed at 56 MSPS due to limitations of the DAC-FPGA interface. Performance is obviously below predicted results. SER never exceeds about 15 dB, indicating a proportional noise source at about 20% of input power. SER also begins falling off much sooner than

expected, indicating a fixed-power noise source at about -50dB , independent of VGA gain. The sources of this noise have not been identified.

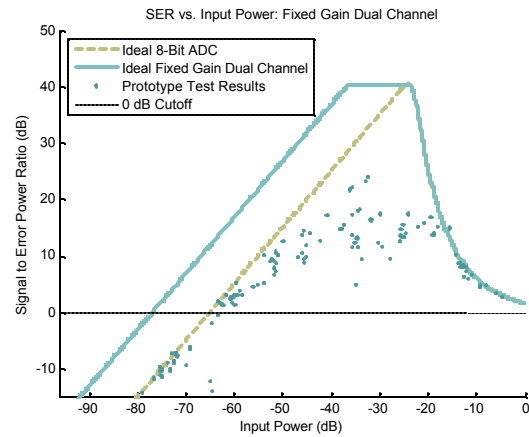


Figure 13: Prototype results, fixed gain dual channel

Test results for the adaptive multichannel system are shown in Figure 14. The same noise sources are still present, but the test shows successful operation of the AGC system at variable gains less than 1.0. The gain controller is therefore operating as expected, with successfully demonstrated operation of the adaptive two-channel AGC system. However, test results are not of adequate fidelity to confirm that the derived gain settings are optimal.

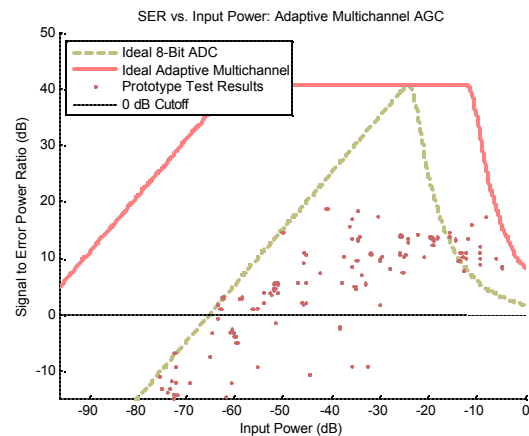


Figure 14: Prototype results, adaptive dual channel

6. CONCLUSIONS

Two-channel AGC systems offer significantly improved performance for signals with rapid changes in input signal power, by effectively allowing the simultaneous selection of both conservative and aggressive safety margins. For all change rates $s_A > 3\text{ dB}$, SER can be improved by at least 6 dB. While the same types of performance increase are provided by full multichannel AGC systems, the new topology offers almost as much improvement for a

significantly smaller increase in system complexity. Furthermore, the addition of simple but effective data-characterizing algorithms allows both single- and two-channel AGC systems to detect and adapt to changes in input signal PDF by applying the most appropriate pre-derived set of gain coefficients.

Furthermore, the functional prototype shows that the concept of a two-channel automatic gain control system can be implemented in hardware with very high sampling rates.

Special thanks go to The Aerospace Corporation's Corporate University Affiliates Program for supporting this work.

7. REFERENCES

- [1] Fred H. Irons, Kirk J. Riley, Donald M. Hummels, and Greg A. Friel, "The Noise Power Ratio—Theory and ADC Testing," *IEEE Transactions on Instrumentation and Measurement*, Vol. 49, No. 3, pp. 659-665, June 2000.
- [2] Masayuki Iwamatsu. "Analog-to-digital conversion circuit," U.S. Patent no. 4851842. July 25, 1989.
- [3] Wolfgang Oberhammer et al. "Dynamic range extension of wideband receiver," U.S. Patent no. 6333707. December 25, 2001.
- [4] C. Lee Francis. "Large dynamic range digitizing apparatus and method," U.S. Patent no. 6556328. September 3, 2002.
- [5] Jiren Yuan. "Floating-point analog-to-digital converter," U.S. Patent no. 6317070. November 13, 2001.
- [6] Lauri Sumansen. "Pipeline Analog-to-digital Converters for Wide-Band Wireless Communications." Ph.D. Dissertation, Helsinki University of Technology Electronic Circuit Design Laboratory. December 13, 2002.
- [7] Brian L. Fox. "Analysis and Dynamic Range Enhancement of the Analog-to-Digital Interface in Multimode Radio Receivers." Masters thesis, Virginia Polytechnic Institute and State University. February 1997.

8. BIOGRAPHIES



Alexander Utter received a B.S.E. from Harvey Mudd College in 2005. He will continue studies at Stanford University and hopes to eventually pursue research in biomedical electronics and MEMS devices. Alexander is a member of Tau Beta Pi.



Henry Chen received a B.S.E. from Harvey Mudd College in 2005. He is currently working as a Systems Engineer at Raytheon and will continue his studies at USC. Henry hopes to work in the areas of digital systems and/or systems management.



Shane Ouchi graduated in 2005 with a B.S.E. from Harvey Mudd College and a B.A. in Mathematical Economics from Pitzer College. He is currently working at Raytheon and pursuing a master's at USC.



David Money Harris is an Associate Professor of Engineering at Harvey Mudd College. David received his Ph.D. from Stanford University in 1999 and his B.S. and M.Eng. degrees from MIT in 1994. His research interests include high speed CMOS VLSI design and computer arithmetic. He is the author or coauthor of CMOS VLSI Design: A Circuits and Systems Perspective, Logical Effort, and Skew-Tolerant Circuit Design. He holds seven patents, has written numerous papers, and has designed chips at Sun Microsystems, Intel, Hewlett-Packard, and Evans & Sutherland. When he is not teaching or building chips, David enjoys mountain climbing and flying his Cessna.



Samuel S. Osofsky received his B.S. degree in Engineering from Harvey Mudd College in 1985, and his M.S. and Ph.D. degrees in Electrical Engineering from the University of California, Berkeley, in 1987 and 1991, respectively. Dr. Osofsky has been a member of the technical staff of The Aerospace Corporation for the past 14 years. His current position is Associate Director of the Communication Electronics Department. He has participated and led projects concerning the design, analysis, and space qualification of power amplifiers, the development of a pulsed-IV/S-parameter test station, and numerous space-hardware failure investigations. His professional interests include measurements of microwave systems, microwave systems, fiber-optic communications, and steam locomotives.



Amanda Rainer is expected to receive a B.S.E. from Harvey Mudd College in 2006. She recently participated in a CRA-W DMP sponsored research experience at Carnegie Mellon University. She intends to attend graduate school beginning in fall 2006.



Keane Kaneakua is expected to receive a B.S.E. from Harvey Mudd College in 2006. He is currently an intern at Environet Inc and hopes to pursue a M.Eng. degree at the University of Hawaii.



Chris Prounh is expected to receive a B.S. from Harvey Mudd College in 2006. He is currently interning as a Systems Engineer at Raytheon and plans to continue his studies at USC. When he is not studying, Chris enjoys weight lifting and billiards.